Validation of ash optical depth and layer height retrieved from passive satellite sensors using EARLINET and airborne lidar data: The case of the Eyjafjallajökull eruption.

Dimitris Balis[1], Maria-Elissavet Koukouli[1], Nikolaos Siomos[1], Spyridon Dimopoulos[1], Lucia Mona[2], Gelsomina Pappalardo[2], Franco Marenco[3], Lieven Clarisse[4], Lucy J. Ventress[5], Elisa Carboni[6], Roy G. Grainger[6], Ping Wang[7], Gijsbert Tilstra[7], Ronald van der A[7], Nicolas Theys[8] and Claus Zehner[9]

[1]*Laboratory of Atmospheric Physics, Aristotle University of Thessaloniki, Greece, *Email:balis@auth.gr*

[2]*Consiglio Nazionale delle Ricerche, Istituto di Metodologie per l'Analisi Ambientale (CNR-IMAA), Tito Scalo, Potenza, Italy*

[3]*Met Office, Exeter, United Kingdom*

[4]*Université Libre de Bruxelles, Brussels, Belgium*

[5]*National Centre for Earth Observation, Atmospheric, Oceanic and Planetary Physics, University of Oxford, United Kingdom*

[6]*COMET, Atmospheric, Oceanic and Planetary Physics, University of Oxford, United Kingdom*

[7]*Royal Netherlands Meteorological Institute (KNMI), De Bilt, The Netherlands*

[8]*Belgian Institute for Space Aeronomy (IASB-BIRA), Bruxelles, Belgium*

[9]*European Space Agency, ESRIN, Frascati, Italy*

Abstract

The vulnerability of the European airspace to volcanic eruptions was brought to the attention of the public and the scientific community by the 2010 eruptions of the Icelandic volcano Eyjafjallajökull. As a consequence of this event ash concentration thresholds replaced the 'zero-tolerance to ash' rule, drastically changing the requirements on satellite ash retrievals. In response to that, ESA funded several projects aiming at creating an optimal *End-to-End System for Volcanic Ash Plume Monitoring and Prediction.* Two of them, namely the SACS-2 and SMASH projects, developed and improved dedicated satellite-derived ash plume and sulphur dioxide level assessments. The validation of volcanic ash levels and height extracted from the GOME-2 and IASI instruments on board the MetOp-A satellite is presented in this work. EARLINET lidar measurements are compared to different satellite retrievals for two

eruptive episodes in April and May 2010. Comparisons were also made between satellite retrievals and aircraft lidar data obtained with UK's BAe-146-301 Atmospheric Research Aircraft (managed by the Facility for Airborne Atmospheric Measurements, FAAM) over the United Kingdom and the surrounding regions. The validation results are promising for most satellite products and are within the estimated uncertainties of each of the comparative datasets, but more collocation scenes would be desirable to perform a comprehensive statistical analysis. The satellite estimates and the validation data sets are better correlated for high ash optical depth values, with correlation coefficients greater than 0.8. The IASI retrievals show a better agreement concerning the ash optical depth and ash layer height when compared with the ground-based and airborne lidar data.

1. INTRODUCTION

The Eyjafjallajökull volcano in Iceland (63.63°N, 19.62°W) erupted on the 14th of April 2010 and the ash-loaded plume rose to more than 10 km, deflected to the east by westerly winds [Stohl et al., 2011]. The plume persisted over central Europe from the 15th and the 26th of April 2010, while occasionally extending to southeast Europe [Emeis et al., 2011]. New significant eruptions occurred between May 4th–9th and May 14th–19th 2010 [Gudmudsson et al., 2010]. The first of these phases mainly influenced Western Europe, from Great Britain to the Iberian Peninsula, while the second phase influenced central Europe and the central and eastern Mediterranean on the May 18th–22nd. The last observations of the event were recorded over central Europe on the 25th of May [Gudmundsson et al., 2010]. Although the eruption was a moderate one in terms of volcanic explosivity, due to advection of the volcanic ash plumes, civil aviation was shut down for many days over numerous European countries [Gertisser., 2010] and thus in terms of economic costs was more severe. This resulted in an urgent demand for reliable model forecasts of the vertical and horizontal extent of the ash plume, and for complementary measurements that could be used for nowcasting and forecast verification [Sears et al., 2013]. Following an eruption, Volcanic Ash Advisory Centres (VAAC) distributed around the globe give instructions to civil aviation in order avoid potential hazards [e.g. Guffanti et al., 2010]. Considering the large social and economic impact of any decision, the provided guidelines should be reliable, verifiable and should use all available scientific information [Zehner, 2010]. During the eruption period the European Aerosol Research Lidar Network, EARLINET, responded to this demand with coordinated intensive measurements from ground-based lidar [e.g. Ansmann et al, 2010; 2011; Groß et al., 2011;; Mona et al.,

2012; Papayannis et al., 2012; Perrone et al, 2012; Navas-Guzman et al, 2013; Pappalardo et al, 2013; Trickl et al. 2013; Wiegner et al., 2012], initially by providing quick look images and identification of the volcanic ash layers. This observation campaign provided information on ash height and its vertical extent, as well as an estimation of the ash load in terms of optical depth and mass concentration. In addition, there were a number of dedicated airborne campaigns during the eruption that combined lidar and in-situ measurements of the ash plume [e.g. Marenco et al., 2011; Schumann et al, 2011; Chazette et al., 2012]. The volcanic plume was observed from a variety of satellite instruments such as the Cloud-Aerosol Lidar with Orthogonal Polarization (CALIOP) on board the CALIPSO satellite [Winker et al., 2012] and a number of passive satellite sensors either in low Earth orbit, such as GOME-2/MetopA [e.g. Rix et al., 2012], MODIS/Terra & /Aqua [e.g. Christopher et al., 2012], IASI/MetopA [Carboni et al, 2012], or in geostationary orbit, such as SEVIRI [e.g. Francis et al., 2012]. The World Meteorological Organization organized an intercomparison campaign of twenty two satellite-based volcanic ash retrieval algorithms applied on passive sensors [WMO, 2015]. The intercomparison was based on six selected volcanic eruptions including Eyjafjallajökull. Validation results showed variable agreement with lidar data, depending upon the scene conditions.

In 2012 the European Space Agency (ESA) initiated the project “Satellite Monitoring of Ash and Sulphur Dioxide for the mitigation of Aviation Hazards” (SACS-2) to support authorities and the VAACs during future volcanic events. The project created an optimal end-to-end system for volcanic ash plume monitoring and prediction [Brenot et al., 2014 and http://sacs.aeronomie.be]. The system is based on improved and dedicated satellite-derived ash plume and sulphur dioxide products, followed by extensive validation using satellite and ground-based measurements [Koukouli et al., 2014a; Spinetti et al., 2014]. In this paper, we present validation results for two satellite sensors, GOME-2/MetOp-A and IASI/MetOp-A, concerning the volcanic ash optical depth and ash layer height, using ground and aircraft lidar measurements. The comparisons are restricted to the Eyjafjallajökull eruption period of 2010. In the first section we provide a short description of the satellite data and then a description of the ground-based and aircraft lidar data used as a reference for validation. Then we describe the methodology applied in the comparisons, and the co-location criteria applied. In the second section, we present the comparison results for the different sensors and algorithms, separately for the ground-based and aircraft data. Finally, we discuss the results and summarize our findings.

2. DATA AND METHODOLOGY

2.1 SATELLITE DATA

One of the main tasks of ESA's SACS-2 and SMASH (*Satellite Monitoring of Ash and Sulphur dioxide for the mitigation of aviation Hazards)* projects was to improve and validate the algorithms for the retrieval of ash optical depth and height, using satellite measurements in the infrared and UV-Vis from low Earth orbit sensors. These improvements were based on previous algorithm developments [e.g. de Graaf et al., 2005; Clerbaux et al., 2009; Clarisse et al, 2010, 2013; Gangale et al., 2010; Carboni et al., 2012; Grainger et al., 2013] In this paper we use data from GOME-2 and IASI instruments on board the MetOp-A satellite which covered the whole eruption period of Eyjafjallajökull in 2010. Details of the satellite data are described below.

2.1.1 GOME-2/METOP-A

The Global Ozone Monitoring Experiment-2 (GOME-2) is a visible-ultraviolet scanning spectrometer featuring 4096 channels and 200 polarisation channels in the 240-790 nm spectral range, and featuring a 40x40 km^2 resolution. Data from GOME-2/MetOp-A have been processed by the Royal Netherlands Meteorological Institute (KNMI). The volcanic ash retrieval algorithm includes an estimation of the optical depth of an ash layer based on the Absorbing Aerosol Index (AAI) (Herman et al., 1997; Torres et al., 1998) as well as an estimation of the effective ash layer height. The algorithm is based on look-up tables formed in terms of the AAI, aerosol height, solar zenith angle (SZA), viewing zenith angle (VZA), and relative azimuth angle (RAZI). The AAI is sensitive to atmospheric parameters such as aerosol type, aerosol layer height, and aerosol optical depth (AOD), and to surface height and scattering geometry [de Graaf et al., 2005]. The most dominant parameters are aerosol optical thickness and aerosol layer height. In general, thick aerosol layers produce larger AAI values than thin aerosol layers, while high altitude aerosol layers produce larger AAI values than low lying aerosol layers [Torres et al., 1998; de Graaf et al., 2005]. If the aerosol type, surface albedo, and geometries (SZA, VZA, RAZI) are known, aerosol optical thickness can be calculated using the AAI and aerosol height. The ash layer height is derived using the Fast REtrieval Scheme for Clouds from Oxygen A-band (FRESCO) algorithm [Wang et al., 2008a]. It has been demonstrated that FRESCO can retrieve volcanic ash layer height for optically thick ash plumes [Wang et al., 2012]. The retrieved optical thickness of the ash layer depends on the assumption of aerosol properties used in the look-up tables (LUTs). The volcanic ash

particles are assumed to be spherical and have a bi-modal log-normal size distribution. In our calculations, we used an effective radius of 0.052 µm and effective variance of 1.697 µm for the fine mode, and an effective radius of 0.67 µm and effective variance of 1.806 µm for the coarse mode. The weight of the fine mode was 0.995. Two different a priori assumptions for the refractive index of strongly absorbing volcanic ash were tested, indicated later on as DUST and VOLZ [Volz, 1973; Sinyuk et al., 2003.]

2.1.2 IASI/METOP-A

The Infrared Atmospheric Sounding Interferometer (IASI) is an infrared spectrometer featuring 8461 channels in the 645-2760 cm^{-1} spectral range, with a spectral resolution of 0.25 cm^{-1}. Satellite estimates for the ash optical depth and layer height from IASI/Metop-A have been provided by two institutes, the Université Libre de Bruxelles (ULB) and the University of Oxford (UOXF).

2.1.2.1 ULB algorithm

The dataset provided by the ULB was generated by a LUT-based algorithm described in Moxnes et al. [2014] using two distinct sets of refractive indices: one set provided by Dr. Dan Peters [private communication] based on recent measurements of Eyjafjallajökull ash, and the other set using the basaltic ash refractive index data from Pollack et al, 1973 (referred to as the *Eyja* and *Pollack* datasets respectively). In this paper we show only estimates based on the Eyja refractive index. The index was available with a spectral resolution of 1 cm^{-1}. The algorithm assumes a log-normal particle size distribution with spread 2. The mode radius is retrieved together with the ash optical depth. For this eruption, the ash plume was assumed to be centred at 5 km and no attempt was made to retrieve ash plume height.

2.1.2.2 UOXF algorithm

The datasets provided by UOXF also assume the *Eyja* refractive index, and treat similar the particle size distribution. The algorithmic processing of UOXF resulted in four different products: one characterized as the `iterative' algorithm, which provided ash optical depth and layer height, and three characterized as the `fast' algorithm, which provided ash optical depth for three fixed volcanic ash layer pressures (400 hPa, 600 hPa and 800 hPa). The fast algorithm, based on the method of Walker et al. [2011], carries out a linear retrieval (least squares fit) of the aerosol optical depth, AOD, assuming a fixed plume altitude and effective radius. The algorithm looks for departures in the measured spectra from an expected

background covariance, created from previous IASI measurements containing no volcanic ash. The iterative algorithm is a full optimal estimation retrieval using a forward model based on Radiative Transfer for TOVS (TIROS Operational Vertical Sounder), *RTTOV,* a very fast radiative transfer model for nadir-viewing passive visible, infrared and microwave satellite radiometers. Clear sky radiances from RTTOV are combined with an ash layer in a method described in detail by Thomas et al. [2009a; 2009b]. The iterative scheme then provides probable values of AOD, effective radius and plume altitude [Ventress et al. 2016]. The fast algorithm is used to flag IASI pixels (assuming an AOD threshold defined by the statistics of the scene) for the presence of volcanic ash, at which point the iterative retrieval is carried out on the pixel.

2.2 LIDAR DATA

The validation of the satellite products used lidar measurements from two sources. The first was the intensive ground-based lidar measurements from stations that form the European Research Lidar Network (EARLINET) and the second was the airborne lidar measurements from the UK's BAe-146-301 Atmospheric Research Aircraft managed by the Facility for Airborne Atmospheric Measurements (FAAM). As a matter of fact, the airborne measurements captured larger volcanic ash load than the ground-based network, and this is explained by the fact that the former is a moving platform that was tasked with overflying the areas with large concentrations. The aircraft flights monitored a large area affected by the ash cloud. Meanwhile, for most of the EARLINET stations, the volcanic particles atmospheric content was almost half of that observed in the UK, which was directly downwind from the eruption.

In the next section we provide a brief description of the lidar measurements used as reference data for the validation of the satellite products.

2.2.1 EARLINET DATA

The European Aerosol Research Lidar Network (EARLINET) coordinates ground-based lidar activities on the European continent since 2000, and holds a comprehensive database of European lidar datasets giving information on the horizontal, vertical and temporal distribution of aerosols on a continental scale. Lidar data from the EARLINET network [Pappalardo et al., 2014 and http://www.earlinet.org] were used to validate ash plume height and optical depth. EARLINET was established in 2000 and is the first aerosol lidar network with the main goal of providing data for investigating the aerosol distribution on a continental scale. EARLINET has established certain protocols for the measurements and the quality

control of the systems and the retrieved data, through algorithm [Böckmann et al, 2004, Pappalardo et al, 2004] and system [Matthias et al., 2004a, Freudenthaler et al., 2010, Wandinger et al., 2016), intercomparison campaigns. The network currently includes 27 stations distributed over the European continent. The standard products of EARLINET include aerosol extinction and backscatter profiles. EARLINET data have been widely used for climatological studies [e.g. Matthias et al., 2004b; Amiridis et al., 2005; Giannakaki et al., 2007] as well as for monitoring unusual atmospheric events such as desert dust, biomass burning, pollution episodes, volcanic eruptions and so on. Results have been presented in numerous publications [e.g. Amiridis et al, 2009; Ansmann et al., 2003 ; Guerrero-Rascado et al., 2009; Mamouri et al., 2012; Mattis et al., 2010; Mona et al., 2006 ; Müller et al., 2007 ; Papayannis et al., 2008; Wang et al., 2008b].

A relational database, containing the output of the 4-D analysis of EARLINET data related to the volcanic eruption of 2010, has been set up [Mona et al 2012; Pappalardo et al., 2013] and is freely available on request at http://www.earlinet.org. Information related to the present study involves aerosol backscatter coefficient profiles for each of the ground-based stations [The EARLINET publishing group 2000–2010, 2014], as well as a characterization of the observed layers as pure volcanic or mixed [Pappalardo et al., 2013]. A volcanic aerosol mask was developed [Mona et al., 2012], which involved aerosol typing, back-trajectory analyses and model outputs, used together with the lidar measurements at 1 hour temporal resolution. The data included in the EARLINET database captured the whole Eyjafjallajökull eruptive event over Europe providing geometrical and optical properties of the tropospheric volcanic cloud. The volcanic cloud persisted over central Europe for the whole period at heights of between 3 and 8 km, with maximum load observed on the 16th of April 2010 over Hamburg [Pappalardo et al., 2013]. In our study we only used profiles that were detected as pure volcanic, as these were characterized by the methodology applied in Pappalardo et al., 2013. The list of stations considered for the validation of the satellite products is shown in **Table *I***.

2.2.2 AIRBORNE LIDAR DATA

The satellite products are validated using lidar measurements from six flights by the UK's BAe-146-301 Atmospheric Research Aircraft over the United Kingdom and the surrounding seas in May 2010 [e.g. Marenco et al., 2011; Johnson et al., 2011]. The lidar measurements include aerosol extinction profiles at 355 nm, which in turn provide plume height and layer optical depth. Measurements were integrated to a vertical resolution of 45 m and a temporal resolution of 1 min (corresponding to a typical ~9 km horizontal resolution), and all lidar

profiles have been cloud-screened. An extinction-to-backscatter ratio (lidar ratio) of 60 sr was used for the inversion of lidar signals; this lidar ratio was determined in such a way as to satisfy the constraints of a molecular signal below and above lofted layers. In situ observations were provided by other probes on the aircraft, in particular a three-wavelength nephelometer, a Passive Cavity Aerosol Spectrometer Probe (PCASP) and a Cloud and Aerosol Spectrometer (CAS) optical particle counters; radiative measurements were taken in the visible and infrared. An example of the available aerosol extinction profiles, along with flight altitude and flight track is shown in **Figure *1*** for the 16th of May 2010. The data shown here will be discussed in more detail in the overview of the comparison results. In this paper we mainly used lidar data from May 4th, 5th, 14th, 16th, 17th and 18th 2010 flights, when volcanic ash was detected and satellite data were available. Since the satellite AOD estimates were given at 550 nm we considered scaling the lidar-determined ash layer optical depth to 550 nm using an appropriate Angstrom exponent. According to Pappalardo et al. [2013] and based on EARLINET observations, the Angstrom exponent between 355 and 532 nm ranges between 0.03 and -0.11. So we used an exponent equal to zero, which practically means that the optical depths to be compared were not scaled.

2.3.1. METHODOLOGY FOR THE EARLINET-SATELLITE COMPARISONS

The values of each satellite product have been restricted to an area of variable radius around each EARLINET station, depending on the satellite. The closest measurement in space and time has been selected for each overpass, within the limits set by the collocation criteria shown in ***Table II***. This was compared to the respective layer characterized by EARLINET as volcanic particles. First the spatial collocation criteria have been applied to satellite data and then the temporal ones. The EARLINET relational database for this event contains cases for which two or more volcanic layers are simultaneously observed in the atmospheric column. For these cases the worst correlated layer to the satellite data was excluded from analysis. A summary of the satellite data compared with the EARLINET measurements and the corresponding collocation criteria can be found in **Table *II***. For all the satellite products a comparison of the AOD has taken place. For the satellite products that provided volcanic ash layer height information a comparison of volcanic ash layer height was also performed. The AOD of the EARLINET layers was derived by the layers' integrated backscatter coefficient multiplied by a fixed extinction-to-backscatter ratio with a value of 50 sr^{-1} [Ansmann et al., 2010]. We did not use any Raman lidar measurements since most comparisons were

performed for daytime conditions. An estimated 20% uncertainty on the EARLINET AOD was applied due to the variability of the lidar ratio for volcanic particles, typically between 40 and 60 sr^{-1} [see Pappalardo et al., 2013 and references therein]. For the layer height comparison, the height of the centre of mass provided by the EARLINET database was used, and as estimated layer depth, the distance between the mass centre from the layer top and base was employed. All the satellite ash optical depth products were calculated at 550 nm, apart from the KNMI/GOME2 products which were calculated first at 380 nm and then scaled to 550 nm using appropriate Angstrom exponents provided by the satellite team. In order to convert the infrared optical depth to optical depth at 550 nm, both ULB and UOXF teams used the Eyja refractive indices from Dr. Dan Peters (private communication), with a value of $1.572+i7.5\cdot10^{-6}$ at 530nm. Correspondingly, 532 nm lidar measurements were used in the comparisons.

2.3.2. METHODOLOGY FOR THE AIRCRAFT-SATELLITE COMPARISONS

The airborne lidar data were available on a per flight basis [Koukouli et al., 2014b] and included aerosol extinction profiles that provided ash plume height and ash layer optical depth. The values of these variables were compared with the satellite produced values of ash optical depth and aerosol layer height (where given) examining different collocation criteria corresponding to an area of a radius ranging from 50 km to 200 km (see Table III). The closest satellite value, within the selected spatial criteria, for every flight path location was found and used for the comparisons. Since the overpass times of the satellite data are around 9:30 L.T. and 21:30 L.T., in order to allow for co-location, only spatial criteria where used. None of the available aircraft data were available within 1-2 hours of the overpass time, which was the criterion that provided the best matches when using the EARLINET data. The time difference between satellite and aircraft data was around 5 hours. This fact does not allow a point-to-point comparison of the measurements but the comparisons will mainly highlight whether the ash products from the two measuring systems are consistent. A summary of the satellite data compared against the flight measurements and the corresponding collocation criteria can be found in **Table *III***.

3. RESULTS AND DISCUSSION

3.1 COMPARISON OF ASH OPTICAL DEPTH AND ASH LAYER HEIGHT WITH EARLINET DATA

As shown in **Table *III***, we applied different collocation criteria between the EARLINET lidar measurements and the satellite observations, to investigate which one provides the best

results and a reasonable number of matches. Although during April and May 2010 the EARLINET stations performed a large number of dedicated intensive measurements, the overpass time of the MetOP-A satellite significantly limited the number of collocations. We examined, for each of the collocation criteria, the correlation coefficient between the lidar-determined optical depth of the pure volcanic particles layer and the corresponding satellite estimate. Furthermore, we examined the correlation coefficient between the ash layer height estimated from the lidar measurements and the one retrieved from the satellite algorithms when available [Koukouli et al., 2014b]. In Figure 2 we present scatter plots between EARLINET ash layer optical depth and each satellite ash product for those collocation criteria that showed the largest correlation. The best correlations were found when limiting the matches to within a radius of 100 km from the ground-based lidar and considering measurements with a one-hour difference. When deviating from these criteria, the number of matches increased but the correlation declined. This fact provides an indication of the spatial and temporal representativeness of single lidar profiles. Different colours in these plots correspond to different European regions (see **Table *I***) in order to examine whether the distance from the source and the transport path have an impact on the comparisons.

The GOME-2A comparisons are shown in Figure 2a and 2b with the ”dust” refractive index in the left column and the “Volz” refractive index in the right column. Only twelve collocations were found for the GOME-2 and the EARLINET observations. There is a small correlation between the datasets, ranging between 0.33 and 0.46 for the “dust” and “Volz” products respectively. This limited number of co-locations were given by a radius of 300 km from each ground-based station and within 5 hours. The GOME-2A estimates of the ash layer optical depth are systematically larger than the lidar ones and most of them are larger than 1, although for these cases the lidar data rarely exceed the value 0.5. The large GOME-2 pixel size (80 km x 40 km) and the large search radius (300 km) could partly explain differences with point measurements, like the lidar; however it seems possible that despite the screening of the cloudy events contamination could still be possible from thin clouds in the GOME-2A retrievals, considering the pixel size, which is compared to the point lidar measurement. The lidar data included in the EARLINET database have been thoroughly cloud screened. Between the two GOME-2A products the “Volz” algorithm shows a slightly better correlation coefficient with the ground-based lidars.

The scatter plots of UOXF ash optical depth and collocated EARLINET measurements are presented in Figure 2c and 2d; the plot in the left column corresponds to the iterative

algorithm and the right column corresponds to the "fast" algorithm at a fixed height of 600 hPa, which is consistent with the average height where EARLINET observed volcanic particles. For both algorithms the collocation criteria that provided the best results were a distance from each ground-based station of 100 km and a maximum time difference of one hour. These criteria allowed for almost 20 coincidences. As it can be quickly verified by the results shown in Figure 2c and 2d, the ash AOD extracted from the IASI/MetOpA Oxford iterative algorithm is quite low, with values rarely rising above 0.2, which is consistent with the EARLINET measurements, which show similar AOD levels. There are only two cases showing AOD values larger than 0.2 and these are also consistent with EARLINET, since the lidar data for these two cases show significantly larger values, above 0.4. The correlation coefficient is quite promising at 0.85, however it is based on only 18 coincident measurements. The agreement between IASI and EARLINET estimates is similar for the "fast" algorithm, showing a larger scatter for the low AOD values but potentially less scatter for larger AODs. This larger scatter leads to a smaller correlation coefficient close to 0.78. If we loosen the collocation criteria to 300 km and 3 hours then the correlation coefficient drops significantly to a value of less than 0.5.

In Figure 2e we show comparisons of the ash optical depth from the ULB algorithm with EARLINET estimates. The results are shown for the same collocation criteria applied to UOXF comparisons, i.e. 100 km distance and one hour difference between the observations. The general picture is consistent with the IASI/UOXF datasets, however the number of coincidences decreases to only 13, since the two algorithms have different criteria for considering a retrieval as successful. . The comparisons show a correlation of 0.91, which is the largest found in all comparisons shown in Figure 2, based however on a small number of measurements. **Table *IV*** provides the mean EARLINET and satellite ash optical depths for the coincidences shown in Figure 2, along with the mean bias, the rms of the differences, the correlation coefficient and the slope and intercept of the regression line. The average AOD values of the measurements that meet the collocation criteria are small (less than 0.2) and consistent with each other, showing a small mean bias, except in the case of GOME-2A and when the IASI-UOXF fast algorithm has a fixed height of 800 hPa (not shown in Figure 2), where the satellite data overestimate significantly the ash optical depth. However as it is demonstrated in the rms differences the scatter is quite large and even when the correlation coefficients are good, the slope of the regression line is not close to one. Concerning the IASI retrievals all data sets tend to slightly overestimate the small AOD values and underestimate the high AOD values, while the GOME-2 as said show a systematic overestimation. We have to repeat however that all the statistics are based on a small number of coincidences.

The GOME-2A ash products and the iterative IASI product processed by UOXF provided the height of the ash layer. These heights were compared with the estimates from EARLINET and the results are shown in **Figure *3***. The ash plume height estimated for GOME-2A products and the EARLINET network are compared in Figure 3a. Irrespective of the product and the search radius (not shown here) the comparison is not satisfactory for either of the two algorithms. The GOME-2A-provided height seems to strongly under-estimate the ground-based values, showing a narrower range of values between 1 and 5 km. The ground instruments show a more physical spread of the ash cloud locating it between 2 and 6 km. The comparison of the ash plume height extracted from the IASI/MetopA UOXF iterative algorithm and the one observed by the EARLINET network is shown in **Figure *3***b. It is evident from this figure that the spread of plume heights found by the EARLINET network is higher than those found by the Oxford iterative IASI algorithm leading to rather poor correlations. The estimate of the mean is consistent between the datasets. This fact is demonstrated in the summary **Table *V*** which gives the mean EARLINET and satellite ash plume height estimates. The large scatter bars indicate the variability inherent in both sets of observations. We have to note here that the UOXF-fast algorithm with fixed heights for the ash performs better for 600 hPa, which is consistent with the average heights estimated by the nominal algorithm and the EARLINET data, which range between 3 and 4 km. In all lidar-satellite comparisons there was no indication that there were regions where the agreement between the two datasets is better, due to their proximity to the source. However this conclusion is based, especially for certain regions, on extremely few data.

3.2 COMPARISONS OF ASH OPTICAL DEPTH AND ASH LAYER HEIGHT WITH AIRBORNE LIDAR DATA

During May 2010 there were 12 flights of the UK's BAe-146-301 Atmospheric Research Aircraft [Marenco et al., 2011], and during six of these volcanic ash was detected in the airborne lidar measurements. In order to avoid contamination from cirrus clouds and mixed aerosol layers, we only show comparisons with the satellite data for two flights, during which significant levels of pure ash, not mixed with other aerosol types, were observed by the airborne lidar measurements. The flight that took place on the 16th of May 2010 (see also Figure 1), started at 12:55 U.T. and ended at 18:00 U.T. and the aircraft mostly flew over Scotland and northern England. During this flight most of the ash was observed between 55^{o} and 56^{o}N. The flight that took place on the 17th of May over the Irish and North Sea, started a little earlier at 11:15 U.T. and ended at 16:58 U.T., and most of the ash was observed over the North Sea between

1° and 2°E. As is demonstrated in ***Table III***, we only used spatial criteria to find coincidences between the airborne lidar data and the satellite data of the same day, since both flights were performed in the afternoon, while the satellite overpasses are close to 9:30 U.T. (GOME-2A and IASI) and 21:30 U.T. (IASI only). For GOME-2 we found coincidences only for the 17th of May 2010. The airborne lidar data give a time series of data for each measurement day. As data are not truly coincident with the satellite data (the overpass time being early in the morning and late in the evening whereas flights were near the middle of the day), volcanic plumes have undergone advection between the measurements compared. Looking at the data as a time series it makes it easier to capture differences due to the misplacement of plumes. Therefore we do not show correlation coefficients and scatter plots for the satellite-aircraft comparisons, because these are not truly coincident and thus the estimated statistics did not show a good correlation. This however could be misleading concerning the usefulness of the comparisons and therefore we decided to show and discuss only qualitatively about the spatial consistency between the aircraft and the satellite data.

In ***Figure 4*** we show the comparisons of the satellite ash optical depth and the airborne lidar ash layer optical depth for 550 nm as a function of aircraft time (closest point in space). We also show in the bottom row of ***Figure 4*** (4e and 4f) the flight track for the two flights examined. On the path the actual flight time is indicated, in order to be able to identify the spatial location that corresponds to the footprint of the lidar data. Since the time difference between the flight measurement and the satellite overpass is large what we would actually see from the comparisons is (a) if the aircraft and the satellite observe the plume over the same area and (b) if they observe similar optical depth values. This would occur if the dispersion, or transport, of the plume was not significant during the hours elapsing between the satellite overpass and the aircraft measurement, within the spatial criteria we applied for the comparisons. In the ***Figure 4***a and 4b we show the comparisons between IASI ash optical depth for the iterative and fast algorithm of UOXF versus the ash layer optical depth from the airborne lidar measurements for the 16th of May 2010, where the measurements are shown as function of time in U.T.C. In ***Figure 4e*** and ***4f***, we plot the flight path for the two days (16 and 17 May 2010). Along the path the flight time in U.T.C is posted, while the different colours along the flight path indicate the ash optical depth. As we can see, the satellite data processed with the iterative UOXF algorithm captures the high AODs observed around 14:00 U.T. and between 16:00 and 17:00 U.T. quite well, which is not the case with the peak observed

between 15:00 and 16:00 U.T. Such discrepancies can be expected, considering the time difference between the airborne data and the satellite measurements. In addition, it seems that the background is similar but that some larger values are observed between the ash peaks. The situation is slightly different when examining the comparisons between the aircraft data and the estimates from the UOXF fast algorithm using a fixed height of the ash layer at 600 hPa. In general, the UOXF fast algorithm estimates smaller values (including the background); it captures well the peak observed around 14:00 U.T., overestimates the peak in AOD observed between 15:00 and 16:00 U.T. and it is hard to tell if the smaller peak observed around 17:00 U.T. is well-depicted or not.

In ***Figure 4c***, we present the comparisons between the aircraft data and the estimates from the ULB-Eyja algorithm again for the 16th of May 2010. The satellite estimates follow quite well all peaks observed in the aircraft data, however slightly misplaced. Checking the SEVIRI ash imagery at http://fred.nilu.no for the 16th of May 2010 we observe an almost constant west-east flow of dust throughout the day between 55^{o}N and 58^{o} N, and thus this plume was captured both by the morning and by the evening orbit of IASI, as well as by the aircraft when flying over these latitudes between 14:00 and 16:00 UT. SEVIRI observed a plume after 17:00 UT south of 54^{o} N moving southeast. The early evolution of this plume was captured by the aircraft around 17:00 and its later evolution was captured over the same area by the evening orbit of IASI. This plume evolution can partly explain the displacement observed, since the satellite data are not coincident in time with the aircraft data and the time in x-axis of the plots actually corresponds to different latitude/longitude of the comparisons.

In ***Figure 4d*** we present the corresponding comparisons between the aircraft data and the estimates from the GOME-2 KNMI algorithm for the 17th of May 2010, and in the right hand column of the last row of Figure 4 the corresponding flight path of the aircraft. The GOME-2 results capture the levels of the two AOD peaks observed in the aircraft measurements but fail to capture small scale variability in the AOD and the background levels. As on 17th May the aircraft mainly flew an East-West track (whereas on the 16th it was mainly a North-South track), the comparison is coarser and the same satellite data point is assigned to several airborne measurements, resulting in the horizontal lines in Figure 4d. In these cases we actually compare only the morning orbit (9:30 UT) since GOME-2 is a UV/Vis sensor. SEVIRI images show a southeast movement of the ash plume starting east of the coast of England and going towards the Netherlands. The east-west motion of the aircraft over the sea captured this plume between 14:30 and 15:00, and GOME-2 observed this plume over the

same area in the morning. Before 14:30 UT the aircraft was flying over land and did not observe any significant ash, so when compared with the morning observations of GOME-2 and considering the pixel size of GOME-2 and the collocation criteria applied, these measurements are actually compared with satellite data over the sea. Considering the large time difference between the flight and GOME-2 overpass and the much larger pixel size of GOME-2, compared to IASI, it is remarkable that the satellite data can quantitatively capture the ash optical depth in the greater flight area. **Table *VI*** summarizes the mean AODs values observed from the aircraft lidar and each of the satellite products examined.

Finally, in **Figure *5*** we present the comparisons of the ash layer height observed from the aircraft measurements and the corresponding effective ash height estimated from the UOXF-iterative algorithm based on IASI (Figure 5a) and the KNMI algorithm based on GOME-2 (Figure 5b). Considering the constraints induced by the collocation criteria, both algorithms show very good agreement with the corresponding heights estimated from the airborne lidar data in most of the collocations, with the ash height mainly ranging between 3 and 5 km. **Table *VII*** summarizes the mean ash layer height observed from the aircraft measurements and each satellite product examined.

4. SUMMARY AND CONCLUSIONS

The main aim of this work is to present a first attempt to validate improved and dedicated satellite-derived ash plume level assessments as part of the European Space Agency initiatives, in order to create an optimal "*End-to-End System for Volcanic Ash Plume Monitoring and Prediction* systems". The data used as reference for the validation were not part of a specifically designed validation campaign, which explains the small number of coincident data found. The results shown are complementary to other satellite volcanic ash products, e.g. from SEVIRI (Prata and Prata, 2012, Clarisse and Prata, 2015, WMO, 2015). Different aerosol optical depth and ash plume height estimations from GOME2/MetopA and IASI/MetopA have been assessed against collocated ground-based and airborne Lidar data for the 2010 eruptions of the Icelandic volcano Eyjafjallajökull. The GOME2/MetopA measurements have been analysed by the Royal Netherlands Meteorological Institute (KNMI) and the IASI/MetopA observations by both the Université Libre de Bruxelles (ULB) and the University of Oxford (UOXF). Different algorithm versions and parameters were examined and inter-compared. Both aerosol optical depth and ash plume height satellite estimates were compared with European Aerosol Research Lidar Network [EARLINET] lidar measurements

and the UK's BAe-146-301 Atmospheric Research Aircraft flying over the UK during the eruptive period.

- The KNMI GOME2 AOD over-estimates the ground-based values, showing quite high values for cases where the LIDAR sees a low AOD. As a result, the *dust* algorithm shows relatively low correlation coefficients of between 0.25 and 0.3 depending on the spatiotemporal search radius, whereas the *Volz* algorithms perform slightly better, with r^2 values ranging between 0.4 and 0.5. The KNMI/GOME2 data seem to suffer from the spatial resolution of the satellite instrument which made the spatial criterion rather too large hence precluding any conclusive comparisons when compared to the aircraft measurements. The agreement between the satellite-derived and airborne lidar effective ash heights differ only by 1 km on the average, indicating a homogenous spread of the plume under the satellite's pixel. The KNMI GOME2 ash plume height comparisons are not satisfactory, irrespective of the search radius, for either of the two algorithms. The satellite ash height values seem to under-estimate the ground-based values, having a very narrow range of values between 1 and 2 km and a mean of 2.07±1.22 km. In comparisons, the ground instruments show a more natural spread between 3 and 6 km with a mean of 3.92±1.22 km. It is highly likely that the large GOME-2 pixel size smooths out any small scale variability of the plume height, otherwise captured by the ground- based single point measurements.
- The Oxford nominal IASI algorithm shows satisfactory AOD correlations against the ground AODs, with coefficients ranging between 0.6 and 0.85, and, even though it provides rather small optical depths, these are of the same order of magnitude as the lidar. The algorithm presents quite good comparisons for the AOD patterns observed with aircraft lidar. The Oxford nominal IASI algorithm ash plume height comparisons do not show any significant correlation with the EARLINET estimates. The satellite estimates have no spread in values compared to the lidar estimates, however both datasets show similar average values, indicating that the satellite estimates can capture the average conditions. The results are better when compared with the aircraft lidar, where it seems that the satellite estimates follow the variability of ash height along the flight route; however they slightly underestimate the height values with a mean of 3.73±1.45km [compared to the aircraft mean of 4.30±2.00 km].
- The Oxford fast IASI algorithm also provides the same order of magnitude AOD estimates as the ground lidar, with the narrower spatio-temporal choice providing the most promising results: the 400 hPa product has a correlation of around 0.7 and the 800 hPa

product a correlation of around 0.8. The Oxford fast IASI algorithm shows a very good agreement with the aircraft lidar, where the 600 hPa product, that corresponds to the actual plume height, appears to perform best.

- The ULB AOD estimates are the most promising, showing the highest correlation coefficients, ranging between 0.74 and 0.91, depending on the spatio-temporal criterion chosen. This is also valid when we examine the ULB IASI – aircraft comparisons. The ULB IASI algorithm shows a very good agreement, both with respect to the absolute AOD values and with AOD features during the flight shown. The actual absolute AOD maxima are also represented best by this product.

Concluding, we note that, depending on the careful choice of collocation criteria, the satellite algorithms investigated here can observe the ash optical depth and plume height for large enough eruptions to a satisfactory degree. The results shown in this study are in line with the main finding of the dedicated WMO intercomparison study [2015] concerning the agreement between satellite ash products and validation data sets (for AOD correlations between 0.4 and 0.6 and ash layer height agreement within 2km) and in some cases the results shown here show better statistics. However, in order to quantify the levels of accuracy of the satellite assessments, eruptions with strong ash plumes need to be included in this type of validation exercise, since there were too few co-location scenes for most satellite products for the Eyjafjallajökull and Grimsvötn 2010 and 2011 eruptions, as examined in the course of the SACS/SMASH ESA projects. This validation study highlights the need for dedicated validation campaigns during volcanic eruptions. For future eruptions it could be recommended to fly instrumented aircraft along the satellite orbit in order to optimize the colocations between satellite data and aircraft-based observations. It is recognised however that this would be a difficult campaign to plan, given that it is not possible to make long-term predictions of the eruptions.

Acknowledgements

The comparison study was funded by the European Space Agency in the frame of the “Satellite Monitoring of Ash and Sulphur dioxide for the mitigation of Aviation Hazards”-SACS-2 project. The financial support for EARLINET in the ACTRIS Research Infrastructure Project by the European Union’s Horizon 2020 research and innovation program under grant agreement n. 654169 and previously under grant agreement n. 262254 in the 7thFramework Program

(FP7/2007-2013) is gratefully acknowledged. The UK's BAe-146-301 Atmospheric Research Aircraft flown by Directflight Ltd and managed by the Facility for Airborne Atmospheric Measurements (FAAM), which a joint entity of the Natural Environment Research Council (NERC) and the Met Office. L.C. is a research associate with the Belgian F.R.S.-FNRS. LJV was funded through the NERC National Centre for Earth Observation. RGG and EC were supported by the NERC Centre for Observation and Modelling of Earthquakes, Volcanoes, and Tectonics (COMET).

References

Ansmann, A., et al., (2003), Long-range transport of Saharan dust to northern Europe: The 11-16 October 2001 outbreak with EARLINET, Journal of Geophysical Research, 108, 4783, doi: 10.1029/2003JD003757.

Ansmann, A., et al. (2010), The 16 April 2010 major volcanic ash plume over central Europe: EARLINET lidar and AERONET photometer observations at Leipzig and Munich, Germany, Geophys. Res. Lett., 37, L13810, doi:10.1029/2010GL043809.

Ansmann, A., et al. (2011), Ash and fine-mode particle mass profiles from EARLINET-AERONET observations over central Europe after the eruptions of the Eyjafjallajökull volcano in 2010, J. Geophys. Res., 116, D00U02, doi:10.1029/2010JD015567.

Amiridis V., D. Balis, S. Kazadzis, A. Bais, E. Giannakaki, A. Papayannis and C. Zerefos, (2005), Four years aerosol observations with a Raman lidar at Thessaloniki, Greece in the framework of EARLINET, J. Geophys. Res., Vol. 110, D21203, doi:10.1029/2005JD006190.

Amiridis, V., Balis, D. S., Giannakaki, E., Stohl, A., Kazadzis, S., Koukouli, M. E., and Zanis, P., (2009), Optical characteristics of biomass burning aerosols over Southeastern Europe determined from UV-Raman lidar measurements, Atmos. Chem. Phys., 9, 2431-2440, doi:10.5194/acp-9-2431-2009.

Brenot, H., et al., (2014), Support to Aviation Control Service (SACS): an online service for near-real-time satellite monitoring of volcanic plumes, Nat. Hazards Earth Syst. Sci., 14, 1099-1123, doi:10.5194/nhess-14-1099-2014.

Böckmann, C., U. Wandinger, A. Ansmann, et al., (2004), Aerosol lidar intercomparison in the framework of EARLINET: Part II-Aerosol backscatter algorithms, Applied Optics 43, 977-989.

Carboni, E., Grainger, R., Walker, J., Dudhia, A., and Siddans, R. (2012), A new scheme for sulphur dioxide retrieval from IASI measurements: application to the Eyjafjallajökull eruption of April and May 2010, Atmos. Chem. Phys., 12, 11417-11434, doi:10.5194/acp-12-11417-2012.

Chazette, P., Dabas, A., Sanak, J., Lardier, M., and Royer, P.: French airborne lidar measurements for Eyjafjallajökull ash plume survey, Atmos. Chem. Phys., 12, 7059-7072, doi:10.5194/acp-12-7059-2012, 2012.

Christopher, S. A., N. Feng, A. Naeger, B. Johnson, and F. Marenco (2012), Satellite remote sensing analysis of the 2010 Eyjafjallajökull volcanic ash cloud over the North Sea during 4–18 May 2010, J. Geophys. Res., 117, D00U20, doi:10.1029/2011JD016850.

Clarisse, L., Hurtmans, D., Prata, A. J., Karagulian, F., Clerbaux, C., Mazière, M. D. and Coheur, P.-F., (2010), Retrieving radius, concentration, optical depth, and mass of different types of aerosols from high-resolution infrared nadir spectra, Appl. Opt., 49, 3713-3722, doi: 10.1364/AO.49.003713.

Clarisse, L., Coheur, P.-F., Prata, F., et al., (2013), A unified approach to infrared aerosol remote sensing and type specification, Atmos. Chem. Phys., 13, 2195-2221, doi:10.5194/acp-13-2195-2013.

Clarisse, L and F. Prata (2015), Infrared sounding of volcanic ash, in Volcanic Ash: Methods of observation and monitoring (eds S. Mackie, K. Cashman, A. Rust, H. Ricketts and I.M. Watson), in press

Clerbaux, C., Boynard, A., Clarisse, L., et al., (2009), Monitoring of atmospheric composition using the thermal infrared IASI/MetOp sounder, Atmos. Chem. Phys., 9, 6041-6054, doi:10.5194/acp-9-6041-2009.

Gangale, G., A. J. Prata, and L. Clarisse (2010), The infrared spectral signature of volcanic ash determined from high spectral resolution satellite measurements, Remote Sens. Environ.,114, 414–425, 10.1016/j.rse.2009.09.007.

Giannakaki, E., Balis, D. S., Amiridis, V., and Kazadzis, S., (2007), Optical and geometrical characteristics of cirrus clouds over a Southern European lidar station, Atmos. Chem. Phys., 7, 5519-5530, doi:10.5194/acp-7-5519-2007.

de Graaf, M., P. Stammes, O. Torres, and R. B. A. Koelemeijer (2005), Absorbing Aerosol Index: Sensitivity analysis, application to GOME and comparison with TOMS, J. Geophys. Res., 110, D01201, doi:10.1029/2004JD005178.

Grainger, R. G., D. M. Peters, G. E. Thomas, A. Smith, R. Siddans, E. Carboni, and A. Dudhia (2013), Measuring volcanic plume and ash properties from space, in remote sensing of volcanoes and volcanic processes: Integrating observation and modelling, Geol. Soc. Spec. Publ., 380, doi:10.1144/SP380.7.

Emeis, S., Forkel, R., Junkermann, W., Schäfer, K., Flentje, H., Gilge, S., Fricke, W., Wiegner, M., Freudenthaler, V., Groβ, S., Ries, L., Meinhardt, F., Birmili, W., Münkel, C., Obleitner, F., and Suppan, P.: Measurement and simulation of the 16/17 April 2010 Eyjafjallajökull volcanic ash layer dispersion in the northern Alpine region, Atmos. Chem. Phys., 11, 2689-2701, doi:10.5194/acp-11-2689-2011, 2011.

Francis, P. N., M. C. Cooke, and R. W. Saunders (2012), Retrieval of physical properties of volcanic ash using Meteosat: A case study from the 2010 Eyjafjallajökull eruption, J. Geophys. Res., 117, D00U09, doi:10.1029/2011JD016788.

Freudenthaler, V., et al., (2010), EARLI09 – direct intercomparison of eleven EARLINET lidar systems, in: Proceedings of the 25th International Laser Radar Conference, St. Petersburg, Russia, 5–9 July, 891–894.

Gertisser R., (2010), Eyjafjallajökull causes widespread disruption to European air traffic, Geol. Today, 26, 94-95

Groß, S., V. Freudenthaler, M. Wiegner, J. Gasteiger, A. Geiß, and F. Schnell (2011), Dual-wavelength linear depolarization ratio of volcanic aerosols: lidar measurements of the Eyjafjallajökull plume over Maisach, Germany, Atmos. Environ., 48, 85-96, doi: 10.1016/j.atmosenv.2011.06.017.

Gudmundsson, M. T., R. Pedersen, K. Vogfjörd, B. Thorbjarnardóttir, S. Jakobsdóttir, *and* M. J. Roberts (2010), Eruptions of Eyjafjallajökull Volcano, Iceland, Eos Trans. AGU, 91(21), 190–191, *doi:*10.1029/2010EO210002.

Guerrero-Rascado, J. L., Olmo, F. J., Avilés-Rodríguez, I., Navas-Guzmán, F., Pérez-Ramírez, D., Lyamani, H., and Alados Arboledas, L., (2009), Extreme Saharan dust event over the southern Iberian Peninsula in September 2007: active and passive remote sensing from surface and satellite, Atmos. Chem. Phys., 9, 8453-8469, doi:10.5194/acp-9-8453-2009.

Guffanti M., D.J. Schneider, K.L. Wallace, T. Hall, D.R. Bensimon and L.J. Salinas (2010), Aviation response to widely dispersed volcanic ash and gas cloud from the August 2008 eruption of Kasatochi, Alaska, USA, J. Geophys. Res., 115, D00L19, doi:10.1029/2010JD013868.

Herman, J. R., Bhartia, P. K. , Torres, O. , Hsu, C. , Seftor, C., and Celarier, E., (1997), Global distributions of UV-absorbing aerosols from Nimbus 7/TOMS data, J. Geophys. Res., 102(D14), 16,911–16,922, doi:10.1029/96JD03680

Johnson, B., et al. (2012), In situ observations of volcanic ash clouds from the FAAM aircraft during the eruption of Eyjafjallajökull in 2010, J. Geophys. Res., 117, D00U24, doi:10.1029/2011JD016760

Koukouli, M. E., L. Clarisse, E. Carboni, et al., (2014a), Intercomparison of Metop-A SO2 measurements during the 2010-2011 Icelandic eruptions, Annals in Geophysics, Vol 57, Fast Track 2, http://dx.doi.org/10.4401/ag-6613.

Koukouli, M. E., et al. (2014b), SACS2/SMASH Validation Report on the Eyjafjallajökull & Grímsvötn Eruptions, http://sacs.aeronomie.be/Documentation/LAP-AU.T.H-SACS-ValidationReport_FINAL.pdf , last accessed: Thursday, April 28, 2016.

Levelt P.F., et al., (2006), The Ozone Monitoring Instrument, IEEE Trans. Geosc. Rem. Sens., 44 (5), 1093-1101.

Mamouri, R. E., Papayannis, A., Amiridis, V., Müller, D., Kokkalis, P., Rapsomanikis, S., Karageorgos, E. T., Tsaknakis, G., Nenes, A., Kazadzis, S., and Remoundaki, E., (2012), Multi-wavelength Raman lidar, sun photometric and aircraft measurements in combination with inversion models for the estimation of the aerosol optical and physico-chemical properties over Athens, Greece, Atmos. Meas. Tech., 5, 1793-1808, doi:10.5194/amt-5-1793-2012.

Matthias V., J. Bösenberg, V. Freudenthaler, A. Amodeo, D. Balis, A. Chaikovsky, G. Chourdakis, A. Comeron, A. Delaval, F. de Tomasi, R. Eixmann, A. Hågård, L. Komguem, S. Kreipl, R. Matthey, I. Mattis, V. Rizi, J.A. Rodriguez, V. Simeonov, X. Wang, (2004a), Aerosol lidar intercomparison in the framework of the EARLINET project. 1. Instruments, Appl. Opt. 43, N. 4, 961-976.

Matthias V., D. Balis, J. Bösenberg, R. Eixmann, M. Iarlori, L. Komguem, I. Mattis, A. Papayannis, G. Pappalardo, M.R. Perrone and X. Wang, (2004b), Vertical aerosol distribution over Europe: Statistical analysis of Raman lidar data from 10 European Aerosol Research Lidar Network (EARLINET) stations, Journal of Geophysical Research-Atmospheres, 109, D18, D18201.

Mattis, I., P. Siefert, D. Müller, M. Tesche, A. Hiebsch, T. Kanitz, J. Schmidt, F. Finger, U. Wandinger, and A. Ansmann, (2010), Volcanic aerosol layers observed with multiwavelength Raman lidar over central Europe in 2008–2009, J. Geophys. Res., 115, D00L04, doi:10.1029/2009JD013472.

Marenco F., B. Johnson, K. Turnbull, S. Newman, J. Haywood, H. Webster and H. Ricketts, (2011), Airborne lidar observations of the 2010 Eyjafjallajökull volcanic ash plume, J. Geophys. Res., 116, D00U05, doi:10.1029/2011JD016396.

Mona L., A. Amodeo, M. Pandolfi and G. Pappalardo, (2006), Saharan dust intrusions in the Mediterranean area: three years of lidar measurements in Potenza, J. Geophys. Res., vol. 111, D16203, doi:10.1029/2005JD006569.

Mona, L., A. Amodeo, G. D'Amico, A. Giunta, F. Madonna, and G. Pappalardo, (2012), Multi-wavelength Raman lidar observations of the Eyjafjallajфkull volcanic cloud over Potenza, Southern Italy, Atmos. Chem. Phys., 12, 2229-2244, doi:10.5194/acp-12-2229-2012.

Moxnes, E. D., N. I. Kristiansen, A. Stohl, L. Clarisse, A. Durant, K. Weber, and A. Vogel (2014), Separation of ash and sulfur dioxide during the 2011 Grímsvötn eruption, J. Geophys. Res. Atmos., 119, 7477–7501, doi:10.1002/2013JD021129.

Müller, D., Mattis, I., Ansmann, A., Wandinger, U., Ritter, C., Kaiser, D., (2007), Multiwavelength Raman lidar observations of particle growth during long-range transport of forest-fire smoke in the free troposphere. Geophys. Res. Lett., 34, L05803, 2006GL027936.

Navas-Guzman, F., D. Müller, J. A. Bravo-Aranda, J. L. Guerrero-Rascado, M. J. Granados-Munoz, D. Perez-Ramirez, F. J. Olmo, and L. Alados-Arboledas, (2013), Eruption of the Eyjafjallajökull Volcano in spring 2010: Multiwavelength Raman lidar measurements of sulphate particles in the lower troposphere. J. Geophys. Res., 118, 1804–1813, doi:10.1002/jgrd.50116.

Pappalardo G., et al., (2004), Aerosol lidar intercomparison in the framework of the EARLINET project. 3. Raman lidar algorithm for aerosol extinction, backscatter and lidar ratio, Appl. Opt., 43. N. 28, 53705385.

Pappalardo G., L. Moma, G. D'Amico, et al., (2013) Four-dimensional distribution of the 2010 Eyjafjallajökull volcanic cloud over Europe observed by EARLINET, Atmos. Chem. Phys., 13, 4429-4450, doi:10.5194/acp-13-4429-2013.

Pappalardo, G., et al., (2014), EARLINET: towards an advanced sustainable European aerosol lidar network, Atmos. Meas. Tech., 7, 2389-2409, doi:10.5194/amt-7-2389-2014.

Papayannis A., et al., (2008), Systematic lidar observations of Saharan dust over Europe in the frame of EARLINET (2000-2002), Journal of Geophysical Research, 113, doi:10.1029/2007JD009028.

Papayannis, A., et al., (2012), Optical properties and vertical extension of aged ash layers over the Eastern Mediterranean as observed by Raman lidars during the Eyjafjallajökull eruption in May 2010, Atmospheric Environment, 48, 56-65, doi:10.1016/j.atmosenv.2011.08.037.

Perrone, M. R., De Tomasi, F., Stohl, A., and Kristiansen, N. I., (2012), Integration of measurements and model simulations to characterize Eyjafjallajökull volcanic aerosols over south-eastern Italy, Atmos. Chem. Phys., 12, 10001-10013, doi:10.5194/acp-12-10001-2012.

Pollack, J., Toon, O. and Khare, B, (1973), Optical properties of some terrestrial rocks and glasses, Icarus, 19, 372-389.

Prata, A.J. and A.T. Prata, (2012), Eyjafjallajökull volcanic ash concentrations determined using Spin Enhanced Visible and Infrared Imager measurements, J. Geophys. Res., doi: 10.1029/2011JD016800

Rix, M., P. Valks, N. Hao, D. Loyola, H. Schlager, H. Huntrieser, J. Flemming, U. Koehler, U. Schumann, and A. Inness, (2012), Volcanic SO_2, BrO and plume height estimations using GOME-2 satellite measurements during the eruption of Eyjafjallajökull in May 2010, J. Geophys. Res., 117, D00U19, doi:10.1029/2011JD016718.

Sears, T. M., G. E. Thomas, E. Carboni, A. J. A. Smith, and R. G. Grainger (2013), SO_2 as a possible proxy for volcanic ash in aviation hazard avoidance, J. Geophys. Res. Atmos., 118, 5698–5709, doi:10.1002/jgrd.50505

Schumann, U., et al., (2011), Airborne observations of the Eyjafjalla volcano ash cloud over Europe during air space closure in April and May 2010, Atmos. Chem. Phys., 11, 2245-2279, doi:10.5194/acp-11-2245-2011.

Sinyuk, A., Torres, O., and Dubovik, O., (2003), Combined use of satellite and surface observations to infer the imaginary part of refractive index of Saharan dust, Geophys. Res. Lett., 30, 1081, doi:10.1029/2002GL016189.

Spinetti C, G. Salerno, T. Caltabiano, et al., (2014), Volcanic SO_2 by UV-TIR satellite retrievals: validation by using ground-based network at Mt. Etna, Annals in Geophysics, Vol 57, http://dx.doi.org/10.4401/ag-6641, Fast Track 2.

Stohl, A., et al., (2011), Determination of time- and height-resolved volcanic ash emissions and their use for quantitative ash dispersion modeling: the 2010 Eyjafjallajökull eruption, Atmos. Chem. Phys., 11, 4333-4351, doi:10.5194/acp-11-4333-2011.

The EARLINET publishing group 2000-2010, Adam, M., Alados-Arboledas, L., Althausen, D., Amiridis, V., Amodeo, A., Ansmann,A., Apituley, A., Arshinov, Y., Balis, D., Belegante, L.,Bobrovnikov, S., Boselli, A., Bravo-Aranda, J. A., Bösenberg,J., Carstea, E., Chaikovsky, A., Comerón, A., D'Amico, G.,Daou, D., Dreischuh, T., Engelmann, R., Finger, F., Freudenthaler,V., Garcia-Vizcaino, D., García, A. J. F., Geiß, A., Giannakaki,E., Giehl, H., Giunta, A., de Graaf, M., Granados-Muñoz, M. J., Grein, M., Grigorov, I., Groß, S., Gruening, C.,Guerrero-Rascado, J. L., Haeffelin, M., Hayek, T., Iarlori, M.,Kanitz, T., Kokkalis, P., Linné, H., Madonna, F., Mamouriat,R.-E., Matthias, V., Mattis, I., Menéndez, F. M., Mitev, V.,Mona, L., Morille, Y., Muñoz, C., Müller, A., Müller, D., Navas-Guzmán, F., Nemuc, A., Nicolae, D., Pandolfi, M., Papayannis,A., Pappalardo, G., Pelon, J., Perrone, M. R., Pietruczuk,A., Pisani, G., Potma, C., Preißler, J., Pujadas, M., Putaud, J.,Radu, C., Ravetta, F., Reigert, A., Rizi, V., Rocadenbosch, F.,Rodríguez, A., Sauvage, L., Schmidt, J., Schnell, F., Schwarz,A., Seifert, P., Serikov, I., Sicard, M., Silva, A. M., Simeonov,V., Siomos, N., Sirch, T., Spinelli, N., Stoyanov, D., Talianu, C.,Tesche, M., De Tomasi, F., Trickl, T., Vaughan, G., Volten, H.,Wagner, F., Wandinger, U., Wang, X., Wiegner, M., and Wilson,K. M.: EARLINET observations related to volcanic eruptions(2000–2010), World Data Center for Climate (WDCC),doi:10.1594/WDCC/EN_VolcanicEruption_2000-2010, 2014.

Thomas, G. E., Poulsen, C. A., Sayer, A. M., Marsh, S. H., Dean, S. M., Carboni, E., Siddans, R., Grainger, R. G. and Lawrence, B. N., (2009a), The GRAPE aerosol retrieval algorithm, Atmos. Meas. Tech., 2, 679-701, doi:10.5194/amt-2-679-2009.

Thomas, G. E., E. Carboni, A.M. Sayer, et al., (2009b), Oxford-RAL Aerosol and Cloud (ORAC): aerosol retrievals from satellite radiometers in Satellite Aerosol Remote Sensing Over Land (Eds: A.A. Kokhanovsky and G. de Leeuw), Springer.

Torres, O., Bhartia, P. K., Herman, J. R., Ahmad, Z., and Gleason, J., (1998), Derivation of aerosol properties from satellite measurements of backscattered ultraviolet radiation: theoretical basis, J. Geophys. Res., 103, D14, http://dx.doi.org/10.1029/98JD00900.

Trickl T., H. Giehl, H. Jaeger, and H. Vogelmann, 35 years of stratospheric aerosol measurements at Garmisch-Partenkirchen: from Fuego to Eyjafjallajokull, and beyond, (2013), Atmos. Chem. Phys., 13, 5205–5225, doi:10.5194/acp-13-5205-2013

Ventress, L.J.; Carboni, E.; Grainger, R.G.; Smith, A. J. Retrieval of ash optical properties form IASI measurements. *Atmos. Chem. Phys,* in prep. (2016)

Volz, F. E., (2973), Infrared optical constants of ammonium sulfate, Sahara dust, volcanic pumice and fly ash, Appl. Opt. 12,564-568.

Walker, J. C., Dudhia, A., and Carboni, E., (2011), An effective method for the detection of trace species demonstrated using the MetOp Infrared Atmospheric Sounding Interferometer, Atmos. Meas. Tech., 4, 1567-1580, doi:10.5194/amt-4-1567-2011.

Wang, P., Stammes, P., van der A, R., Pinardi, G., and van Roozendael, M., (2008a), FRESCO+: an improved O2 A-band cloud retrieval algorithm for tropospheric trace gas retrievals, Atmos. Chem. Phys., 8, 6565-6576, http://dx.doi.org/10.5194/acp-8-6565-2008.

Wang, P., O. N.E. Tuinder, L. G. Tilstra, M. de Graaf and P. Stammes, (2012), Interpretation of FRESCO cloud retrievals in case of absorbing aerosol events, Atm. Chem. Phys., doi:10.5194/acp-12-9057-2012.

Wang X., A. Boselli, L. D'Avino, G. Pisani, N. Spinelli, A. Amodeo, A. Chaikovsky, M. Wiegner, S. Nickovic, A. Papayannis, M.R. Perrone, V. Rizi, L. Sauvage and A. Stohl, (2008b), Volcanic dust characterization by EARLINET during Etna's eruptions in 2001-2002, Atmospheric Environment ,42, 893–905.

Wandinger, U., et al., (2016), EARLINET instrument intercomparison campaigns: overview on strategy and results, Atmos. Meas. Tech., 9, 1001-1023, doi:10.5194/amt-9-1001-2016.

Wiegner, M., J. Gasteiger, S. Groß, F. Schnell, V. Freudenthaler, and R. Forkel (2012), Characterization of the Eyjafjallajökull ash-plume: Potential of lidar remote sensing, Physics and Chemistry of the Earth 45-46 (2012) 79-86, doi: 10.1016/j.pce.2011.01.006.

Winker, D. M., Z. Liu, A. Omar, J. Tackett, and D. Fairlie (2012), CALIOP observations of the transport of ash from the Eyjafjallajökull volcano in April 2010, J. Geophys. Res., 117, D00U15, doi:10.1029/2011JD016499.

World Meteorological Organziation (2015) WMO SCOPE-Nowcasting: Meeting on the Intercomparison of Satellite based Volcanic Ash Retrieval Algorithms, Final Report, http://www.wmo.int/pages/prog/sat/documents/SCOPE-NWC-PP2_VAIntercompWSReport2015.pdf, last accessed 2/12/2015

Zehner C., Ed. (2010). Monitoring Volcanic Ash from Space. Proceedings of the ESA-EUMETSAT workshop on the 14 April to 23 May 2010 eruption at the Eyjafjoll volcano, South Iceland. Frascati, Italy, 26-27 May 2010. ESA-Publication STM-280. doi:10.5270/atmch-10-01.

Figure captions

Figure 1. Characteristics of the FAAM flight of 16-5-2010. The flight track coloured with AOD (a), and the flight altitude versus time in UT along with a time-altitude cross section for the aerosol extinction coefficient at 355nm (in Mm^{-1}) measured with the aircraft lidar (b).

Figure 2. Scatter plots between satellite ash optical depth at 550nm and EARLINET ash layer optical depth at 532nm for GOME-2A (a) and (b), IASI-UOXF (c) and (d) and IASI-ULB (el) products. Different colors correspond to different European domains. See Table I for more details.

Figure 3. Scatter plots between satellite ash layer height and EARLINET ash layer height (in km), for GOME-2A (a), and IASI-UOXF (b).

Figure 4. Ash optical depth at 550nm and airborne lidar ash layer optical depth at 355 nm as a function of aircraft time. IASI-UOXF products for the 16th of May 2010 (a(and (b), IASI-ULB products for the 16th of May 2010 (c) and GOME-2A product for the 17th if May 2010 (d). The flight tracks for these two days, colored with AOD are shown in (e) and (f)

Figure 5. Ash layer height and aircraft lidar ash layer height (in km) 355nm as a function of aircraft time,. GOME-2A for 17th of May 2010 (a), and IASI-UOXF for the 16th of May 2010 (b).

Table I. Locations of EARLINET lidar stations, their geographical coordinates and corresponding domain assigned (C: Central Europe, N: North-Central Europe, SW: Iberian Peninsula, SE: Italy-Balkans).

Site	Altitude a.s.l. (m)	Lat. (N)	Long. (E)	Domain
Andøya, Norway	380	69.28	16.01	N
Athens, Greece	200	37.96	23.78	SE
Barcelona, Spain	115	41.39	2.11	SW
Belsk, Poland	180	51.84	20.79	N
Bucharest-Magurele, Romania	93	44.45	26.03	SE
Cabauw, The Netherlands	1	51.97	4.93	N
Evora, Portugal				SW
Garmisch-Partenkirchen, Germany	730	47.48	11.06	C
Granada, Spain	680	37.16	-3.61	SW
Hamburg, Germany	25	53.57	9.97	N
Ispra, Italy	209	45.82	8.63	C
L'Aquila, Italy	683	42.38	13.32	SE
Lecce, Italy	30	40.30	18.10	SE
Leipzig, Germany	100	51.35	12.44	N
Linköping, Sweden	80	58.39	15.57	N
Madrid, Spain	669	40.45	-3.73	SW
Maisach, Germany	515	48.21	11.26	C
Minsk, Belarus	200	53.92	27.60	N
Napoli, Italy	118	40.84	14.18	SE
Neuchâtel, Switzerland	487	47.00	6.96	C
OHP, France	683	43.96	5.71	SW
Palaiseau, France	162	48.70	2.20	N
Payerne, Switzerland	456	46.81	6.94	C
Potenza, Italy	760	40.60	15.72	SE
Sofia, Bulgaria	550	42.67	23.33	SE
Thessaloniki, Greece	60	40.63	22.95	SE

Table II. Collocation criteria examined in the EARLINET-satellite comparisons

Institute	Satellite product	Overpass time	Amount of Data In days	Co-location Criteria	Number of coincidences	Comments
KNMI	GOME2/MetopA	09:30 LT	14	3h & 300km	12	
UOXF	IASI/MetopA-Nominal Algorithm	09:30 LT 21:30 LT	18	1h & 100km	18	
UOXF	IASI/MetopA-Fast Algorithm	09:30 LT 21:30 LT	19	1h & 100km	20	3 fixed heights provided, 400 hPa, 600 hPa & 800 hPa
ULB	IASI/MetopA	09:30 LT 21:30 LT	48	1h & 100km	13	

Table III. Collocation criteria examined in the aircraft-satellite comparisons. The flights were performed between 13:00 and 17:30 U.T..

Institute	Satellite product	Overpass time	Amount of data in days	Co-location Criteria	Number of coincidences	Comments
			Max # 5	**No time constraint**		
KNMI	GOME2/MetopA	09:30 LT	1	100km/200km	64	
UOXF	IASI/MetopA-Nominal Algorithm	09:30 LT 21:30 LT	4	50/100/200km	787	
UOXF	IASI/MetopA-Fast Algorithm	09:30 LT 21:30 LT	4	50/100/200km	732-776	3 fixed heights provided, 400, 600 & 800mbar
ULB	IASI/MetopA	09:30 LT 21:30 LT	5	50/100/200km	463	

Table IV. Statistical mean values and associated standard deviation for the EARLINET and the satellite ash optical depth estimates presented for collocated measurements.

Product	Spatiotemporal criteria	Satellite mean AOD at 550nm	EARLINET mean AOD at 532nm	Bias (SAT-GB)	RMS difference	r	slope	Intercept
GOME-2A, KNMI *dust*	300km & 5h	1.18±0.43	0.19±0.21	0.98	0.41	0.33	0.69	1.05
GOME-2A. KNMI *volz*	300km & 5h	1.17±0.61	0.19±0.21	0.97	0.55	0.46	1.37	0.90
IASI, UOXF nominal	100km & 1h	0.08±0.08	0.12±0.12	-0.04	0.07	0.85	0.53	0.02
IASI, UOXF fast 400hPa	100km & 1h	0.10±0.04	0.12±0.12	-0.01	0.1	0.70	0.21	0.07
IASI, UOXF fast 600hPa	100km & 1h	0.17±0.12	0.12±0.12	0.05	0.08	0.78	0.72	0.08
IASI, UOXF fast 800 hPa	100km & 1h	0.32±0.38	0.12±0.12	0.20	0.28	0.78	2.62	0.02
IASI, ULB	100km & 1h	0.09±0.07	0.14±0.14	-0.04	0.08	0.91	0.43	0.03

Table V. Statistical mean values and associated standard deviation for the EARLINET and the satellite ash plume height estimates.

Product	Spatiotemporal criteria	Satellite mean and standard deviation [km]	EARLINET mean and standard deviation [km]	Mean Bias (SAT-GB) in km	RMS difference in km
IASI, UOXF nominal	100km & 1h	3.4±0.78	3.63±0.95	-0.22	1.39
GOME2/MetOp-A	300km & 5h	2.07±1.22	3.92±1.22	-1.84	2.18

Table VI. Statistical mean values and associated standard deviation for the airborne lidar and the satellite ash optical depth estimates at 550nm presented for collocated measurements.

Institute	Instrument & algorithm	Spatial criteria	Mean Satellite AOD levels	Mean Aircraft AOD Levels	Bias (SAT-AIR)	RMS difference
KNMI	GOME-2/MetOp-A	200km	0.42±0.03	0.23±0.15	0.19	0.26
UOXF	IASI/MetopA Nominal Algorithm	50km	0.28±0.25	0.19±0.16	0.09	0.28
UOXF	IASI/MetopA Fast Algorithm 400hPa	50km	0.20±0.30	0.19±0.16	0.01	0.29
UOXF	IASI/MetopA Fast Algorithm 600hPa	50km	0.23±0.29	0.18±0.15	0.05	0.26
UOXF	IASI/MetopA Fast Algorithm 800hPa	50km	0.30±0.40	0.18±0.16	0.11	0.37
ULB	IASI/MetopA	50km	0.21±0.15	0.25±0.17	-0.04	0.23

Table VII. Statistical mean values and associated standard deviation for the airborne lidar and the satellite ash plume height estimates.

Product	Spatial criteria	Satellite mean and standard deviation [km]	Aircraft mean and standard deviation [km]	Bias (SAT-AIR) in km	RMS difference
IASI/MetOpA, UOXF nominal	50km	3.73±1.45	4.30±2.00	-0.59	2.29
GOME-2-MetOpA, KNMI	200km	5.62±0.54	3.87±1.70	1.75	2.33

1

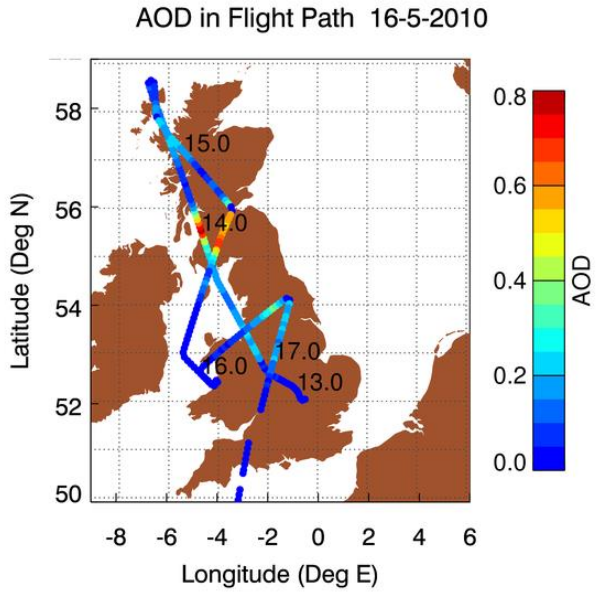

(a)

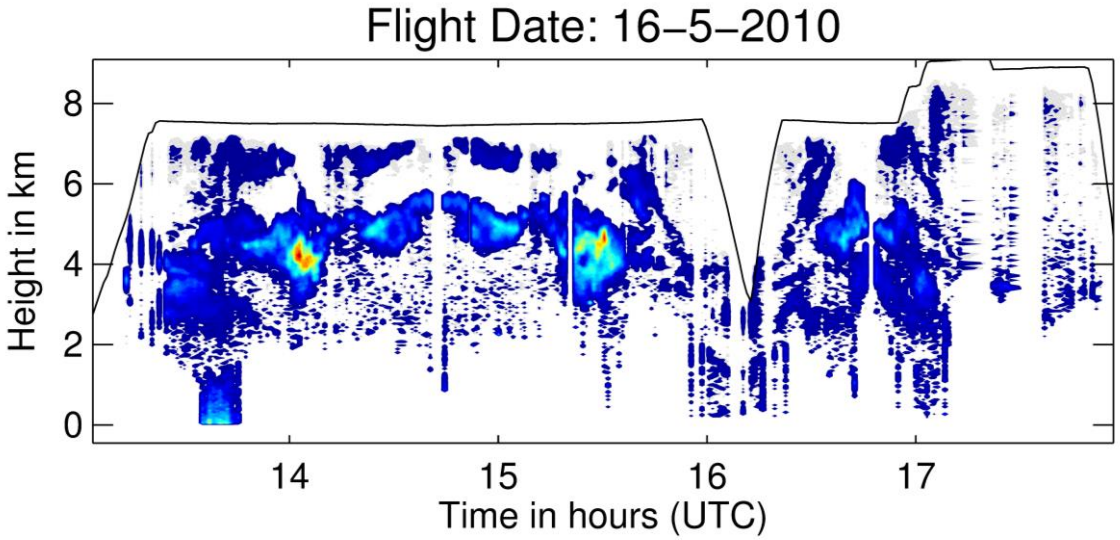

(b)

2 **Figure 1.**

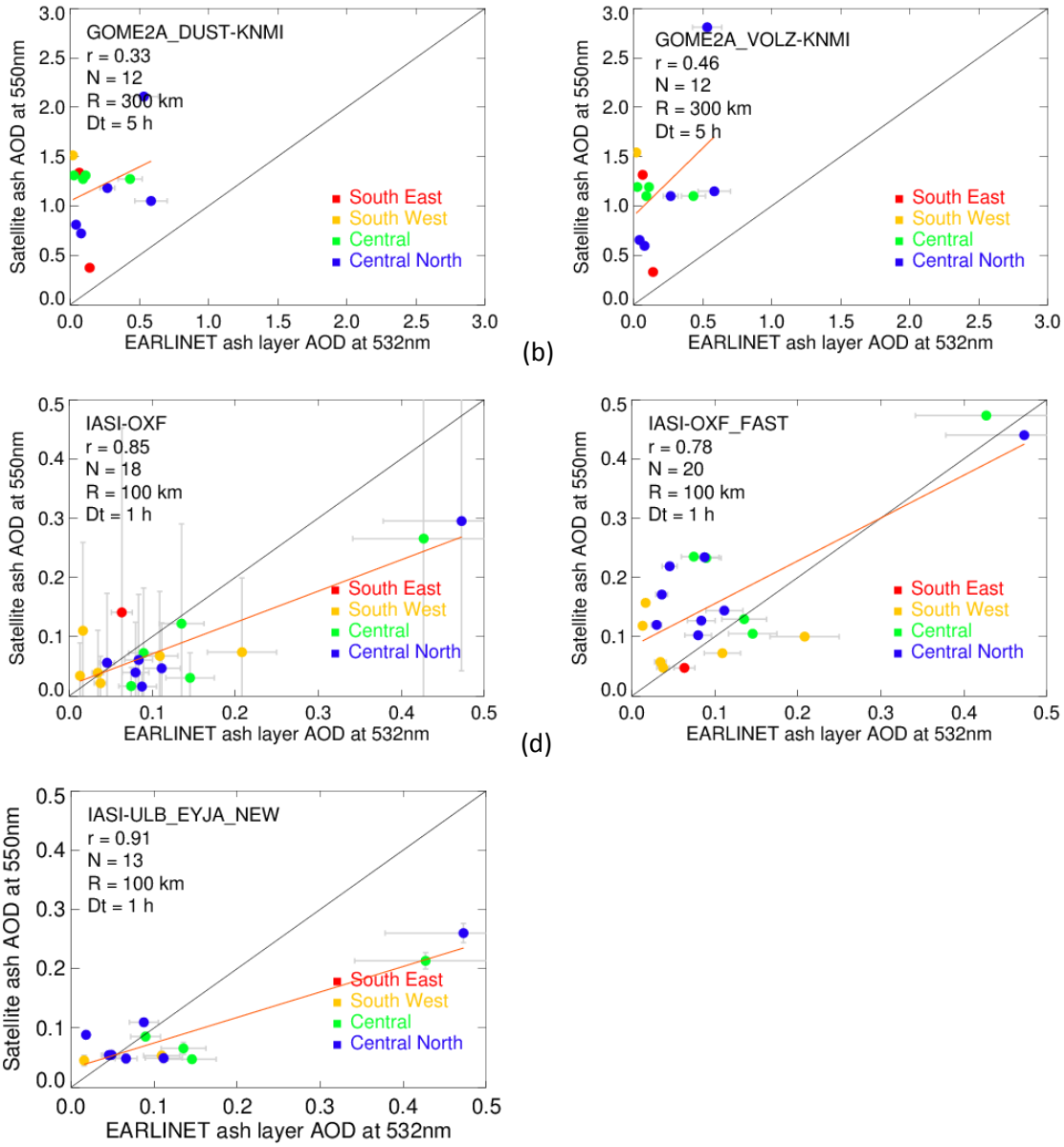
(a)
GOME2A_DUST-KNMI
r = 0.33
N = 12
R = 300 km
Dt = 5 h
Satellite ash AOD at 550nm
EARLINET ash layer AOD at 532nm
South East
South West
Central
Central North
(b)
GOME2A_VOLZ-KNMI
r = 0.46
N = 12
R = 300 km
Dt = 5 h
(c)
IASI-OXF
r = 0.85
N = 18
R = 100 km
Dt = 1 h
(d)
IASI-OXF_FAST
r = 0.78
N = 20
R = 100 km
Dt = 1 h
(e)
IASI-ULB_EYJA_NEW
r = 0.91
N = 13
R = 100 km
Dt = 1 h

Figure 2.

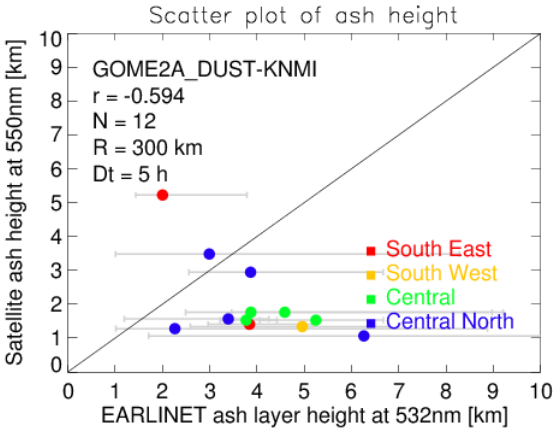
Scatter plot of ash height
GOME2A_DUST-KNMI
r = -0.594
N = 12
R = 300 km
Dt = 5 h
South East
South West
Central
Central North
Satellite ash height at 550nm [km]
EARLINET ash layer height at 532nm [km]

(a)

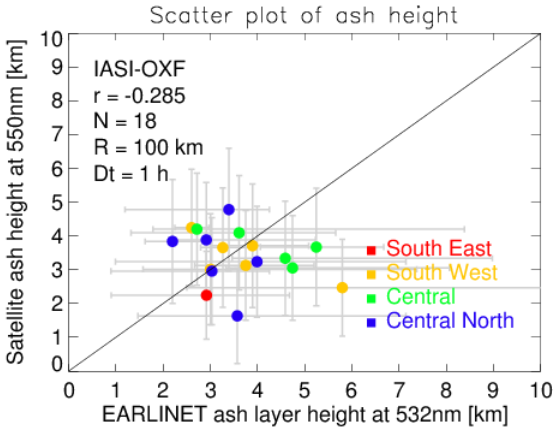
Scatter plot of ash height
IASI-OXF
r = -0.285
N = 18
R = 100 km
Dt = 1 h
South East
South West
Central
Central North
Satellite ash height at 550nm [km]
EARLINET ash layer height at 532nm [km]

(b)

Figure 3.

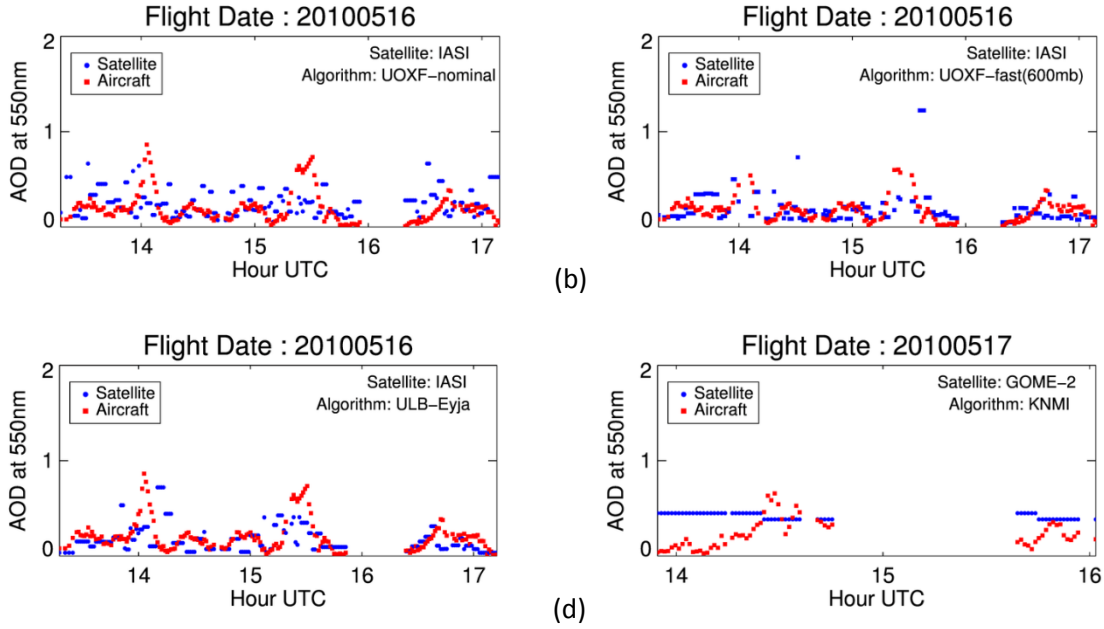
Flight Date : 20100516
Satellite
Aircraft
Satellite: IASI
Algorithm: UOXF−nominal
AOD at 550nm
Hour UTC
(a)
Flight Date : 20100516
Satellite
Aircraft
Satellite: IASI
Algorithm: UOXF−fast(600mb)
AOD at 550nm
Hour UTC
(b)
Flight Date : 20100516
Satellite
Aircraft
Satellite: IASI
Algorithm: ULB−Eyja
AOD at 550nm
Hour UTC
(c)
Flight Date : 20100517
Satellite
Aircraft
Satellite: GOME−2
Algorithm: KNMI
AOD at 550nm
Hour UTC
(d)

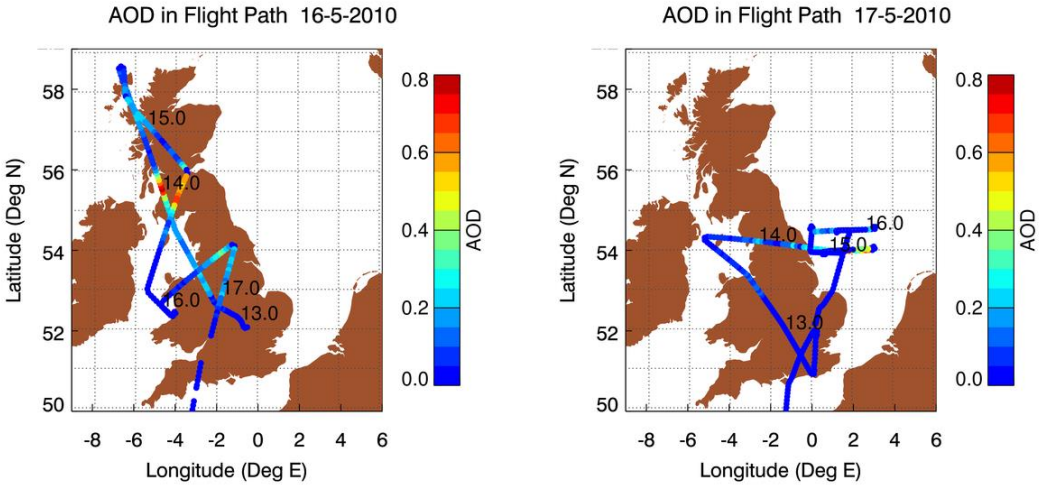
AOD in Flight Path 16-5-2010
Latitude (Deg N)
Longitude (Deg E)
AOD
15.0
14.0
16.0
17.0
13.0
(e)
AOD in Flight Path 17-5-2010
Latitude (Deg N)
Longitude (Deg E)
AOD
14.0
16.0
13.0
(f)

Figure 4.

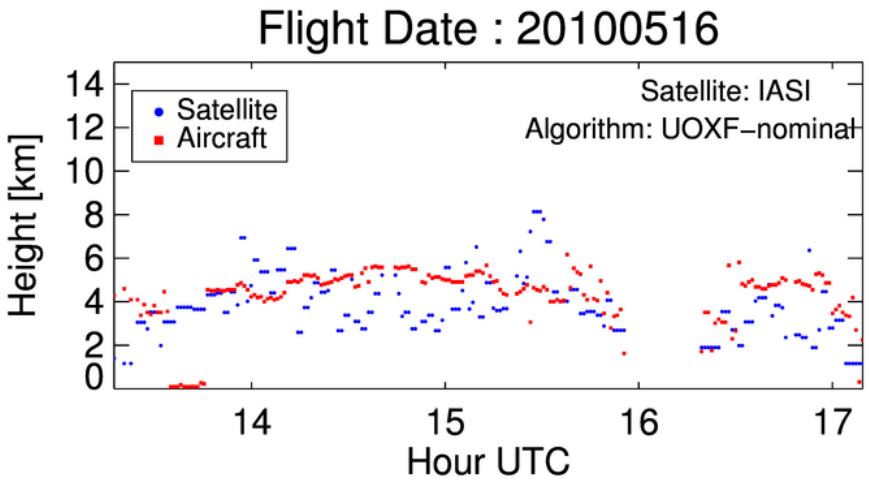
Flight Date : 20100516
Satellite
Aircraft
Satellite: IASI
Algorithm: UOXF−nominal
Height [km]
Hour UTC

(a)

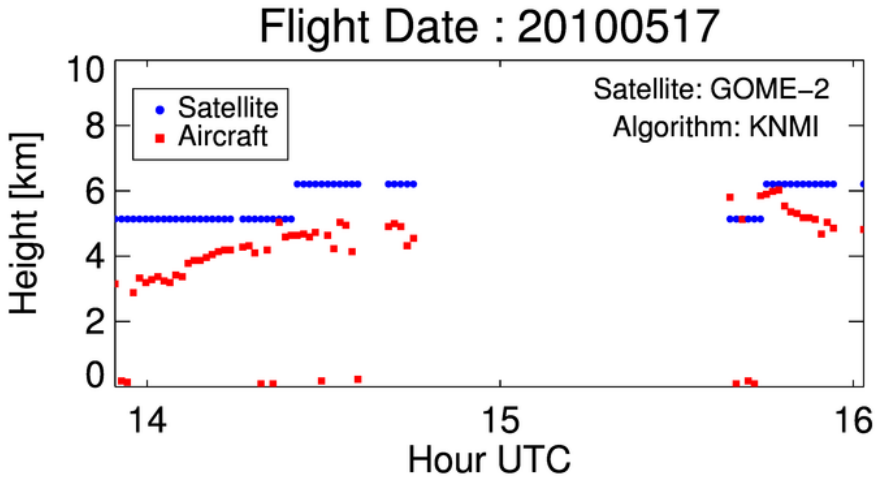
Flight Date : 20100517
Satellite
Aircraft
Satellite: GOME−2
Algorithm: KNMI
Height [km]
Hour UTC

(b)

Figure 5.